Research Article

Inducing the Skinned-oriented Asymmetrical Nanofiltration Membranes via Controlled Evaporation Times in Dry/Wet Phase Inversion Process

Nurul Hannan Mohd Safari and Sabariah Rozali
East Coast Environmental Research Institute, Universiti Sultan Zainal Abidin, Gong Badak Campus, Terengganu, Malaysia

Abdul Rahman Hassan*
East Coast Environmental Research Institute, Universiti Sultan Zainal Abidin, Gong Badak Campus, Terengganu, Malaysia
Faculty of Industrial Design & Technology, Universiti Sultan Zainal Abidin, Gong Badak Campus, Terengganu, Malaysia

Roseley Osman
ANR Synergy Sdn. Bhd., Kuala Lumpur, Malaysia

* Corresponding author. E-mail: rahmanhassan@unisza.edu.my DOI: 10.14416/j.asep.2022.05.007
Received: 10 March 2022; Revised: 10 April 2022; Accepted: 2 May 2022; Published online: 23 May 2022

Abstract
The effect of evaporation time on the fabrication of fine skinned asymmetric polyethersulfone nanofiltration membrane was studied. Nanofiltration experiment and modeling data revealed that the variation of the evaporation time during dry/wet phase inversion process was found to significantly affect the membrane performance and properties. The evaporation times (5 to 25 s) were found to improve the performance and characteristics of the membrane. As good separation performance was achieved, modeling data and morphological analysis discovered that the optimum evaporation time was found to be at 20 s. At these optimal settings, the fabricated membranes demonstrated the finest structural details and morphologies, and the best key properties (r_p, $\Delta x/A_k$ and ζ), which were within the ranges of commercial nanofiltration membranes.

Keywords: Dry/wet phase inversion, Evaporation time, Key properties, Membranes, Nanofiltration

1 Introduction

In the last two decades, polymeric-based membranes gained good interest and have been used for different separation processes [1], [2] and several industrial applications [3], [4]. These trends were driven by the advancement of membranes technology in the aspects of fabrication techniques, modification process, system configuration and the endless efforts from experts towards the achievement of membranes versatility. For gas and liquid separation applications, the membranes have been extensively applied in the industry because of their high selectivity and good mechanical strength [5], [6]. The asymmetric polymeric membranes of reverse osmosis, nanofiltration, ultrafiltration and microfiltration can be produced using the phase inversion process [7]–[10]. A multi-component of a polymeric dope solution is cast and dipped into a specific coagulation bath containing non-solvent as coagulant media, which converts the homogenous solution into a solid membrane [11].

Few techniques of phase inversion have been applied to fabricate the membrane for commercial and laboratory purposes. One of them is phase inversion via dry/wet process, which the evaporation time and other parameters are employed to produce a defect-free/

skinned active layer [12]–[14]. Throughout this process, the prepared membranes possess a thin active layer. The membrane-active skin layer is generated when the steady polymer solution is transformed into the unsteady state in the coagulation step and solvent exchange de-mixing process [11], [15].

In general, the morphologies, structural details and properties were strongly influenced by the membranes making technique, which is the phase inversion process. In addition, the existences of membrane morphologies in asymmetrical membranes are divided into two layers of skin active layer and porous substructures. In the skin layer, the formation of defect-free and skinned-oriented active layer, narrow pores and effective membrane thickness are vital characteristics for high selectivity. Meanwhile, the membrane substructures comprise micro and macro-pores (finger-like, nodular and tears-like) as well as micro and macro-voids and spongy structures which provided the membranes with good mechanical strength for water permeation and solutes flux [16].

All these membrane morphologies played important roles in determining the performance of membranes. Many studies discovered that the changes in morphologies affected the membranes flux n rejection. For example, the existence of microvoids and spongy structures in ALNF membranes strongly contributed to higher permeation and better performances [17]. Meanwhile, the variation of polymer concentration produced a thicker membrane skin layer, large pores size and macrovoids led to the highest rejection and flux rate [18]. Besides, the use of surfactant additives formed the narrow pores width, dense spongy sub-layer and finger-likes structures demonstrated high rejection and good fluxes of BSA and EA proteins [19], [20].

The dry/wet membrane making parameters, such as casting conditions, shear rates, evaporation time and thickness were found to determine the final properties and separation performance of asymmetric membranes. These parameters were proved to strongly affect the membrane rejection efficacy due to the changes in molecular orientation and alterations in the dope rheological conditions [17], [21], [22].

The controlling of dry phase process (evaporation time) and wet phase process was discovered to be a great opportunity for the fabrication of various skin layer thicknesses on the surface of the membrane [23]. After casting, the nascent membrane is undergoing the dry phase state for a certain time of evaporation. During this phase, the polymer molecules are given sufficient time for relaxation, orientation, alignment and rearrangement before the solidification process [24].

The characteristics of the membrane active layer could be determined by the evaporation time. During this process, an inert gas/ambient eliminates the vaporized solvent from the membrane's surface. This mechanism created the higher polymer concentration local region where the spinodal decomposition is directly induced at the outmost of membranes [25]. By manipulation of evaporation time during the dry phase region, the development of a thin active layer could be monitored [26]–[28]. According to a previous report, longer evaporation time produced denser skin layers, which eventually increased the retentions and decreased the fluxes. The formation of these compact layers was caused by the suppression of sub-structures during dry/wet phase inversion process [29].

Nanofiltration membranes are well-known due to their capability for ions separation from water, good multivalent ions and monovalent ions retention [30]. Practically, the high demand for nanofiltration membranes-based separation process worldwide was derived from their advantages of low cost, high flux and good ionic retention [31], [32] as well as better permeation and separation efficacy for liquid state process [12], [33]. Besides, nanofiltration is also applied for water and wastewater treatment [34], pesticides and organic pollutants removal, especially for the production of softened water [35] and fresh potable water as well as divalent and monovalent salts, electrolytes solution [14], [20], [36].

Membrane's structural parameters and properties for nanofiltration can be determined using a theoretical model depending on the membranes process and testing conditions. The effects of evaporation time towards membranes performance were reported by several researchers [26], [27], [29], [37], however, the evolution of membrane parameters, properties and evolutions of morphological structures of nanofiltration membranes at different evaporation time is not yet reported elsewhere and has been ignored despite the facts that this simple step is very important for alteration of membranes structures and properties.

As many studies reported the revision in membrane's performance and properties, the evaporation times are predicted to produce a selective nanofiltration

membrane with narrow pores and fine key properties. Therefore, in this study, the roles of evaporation time during the dry/wet phase inversion process on membrane performances, structural details and key properties were studied via experimental and modeling approaches. In addition, the effect of evaporation time in determining the improved morphological structures in asymmetric nanofiltration membranes was examined.

2 Experimental

2.1 *Materials*

The polymer dopes were formulated from polyethersulfone (PES, Radel A300), N-methyl-2-pyrrolidone and polyvinyl-pyrrolidone, which were used as polymer, solvent and additive, respectively. Methanol, water and distilled water were used as a post-treatment medium, coagulation bath and non-solvent, respectively. Performances of membranes were carried out using NaCl, Na_2SO_4, $MgSO_4$ and $MgCl_2$ for the nanofiltration test, meanwhile neutral solutes with different series of MW (Sigma Aldrich) were used for characterizing structural parameters and properties of membranes [30].

2.2 *Dopes formulations and membrane making*

In order to prepare good formulations, a binary dope component consisting of polymer/solvent undergoes a turbidimetric process. In this step, 100 g of dope will be titrated with water as non-solvent until the polymer solution turns milky. The titration was carried out at room temperature with 84% humidity until changeless cloudy was noticed visually. The method was implemented to get data on cloud point/equilibrium thermodynamics, which consequently defined the equilibrium composition of a ternary system (polymer/solvent/non-solvent).

A new polymeric dope solution was prepared at temperatures of 70 °C. 20.42 wt% of polymer was dissolved into a multi-component formula. Then, the prepared solution was placed in an ultrasonic bath to eliminate air bubbles and kept for 24 h at room temperature. After degassing, the dope solution was cast on a support glass plate with a casting knife. The fabrication was conducted based on dry/wet phase inversion process, under the specific condition as shown in Table 1. The calculation of the shear rate is based on the Equation (1):

$$\text{Shear rate, } \gamma = \frac{v}{g} \quad (1)$$

where v is velocity of casting knife and g is gap setting of casting knife [14], [38].

Table 1: Casting conditions of nanofiltration membranes

Membranes	Shear rate, γ (s^{-1})	Membrane thickness (μm)	Evaporation times (s)
NF25	233.33	150	25
NF20	233.33	150	20
NF15	233.33	150	15
NF10	233.33	150	10
NF05	233.33	150	5

Casting speed = 10 s, Coagulant temperature = 25 °C

During the dry phase, the nascent membranes were undergoing forced-convective evaporation whereby the membrane surface was flushing with nitrogen gas at different evaporation times (Table 1). A nascent skin layer is formed from a region with locally elevated polymer concentration due to a selective loss of highly volatile solvent from the outermost surface of a freshly cast membrane. The underlying region beneath the nascent skin layer remains in a fluid state. Subsequently, the membrane was immersed in coagulant media (water) for 24 h. After that, it was transferred into methanol for another 24 h and followed by a drying process. During the wet phase separation, the bulk of the membrane structure is formed by counter-diffusion of solvents and non-solvents and extraction of the remaining components occurs [39]. The membranes making process via dry/wet phase inversion could be summaries as in Figure 1.

2.3 *Nanofiltration test*

A flat sheet of circular disk NF membrane was cut and underwent a compression process (at 500 kPa) for 1 h. Using a filtration cell (dead-end permeation cell, Model Millipore) and membranes area of 1.39×10^{-3} m^2, the compressed membranes were subjected to pure water permeation and solute separations tests (solutes flux and real rejection) at different transmembrane pressures, which are 300, 350, 400, 450, and 500 kPa.

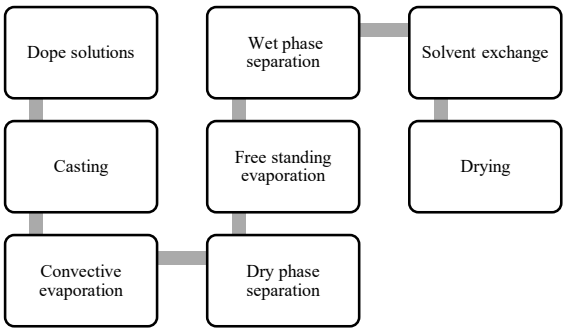

Figure 1: Flow diagram of membranes making via dry/wet phase inversion.

For each experiment run, the permeate samples (20 mL) were collected and weighed for every minute by an electronic balance. All the data are average values from three times of experimental works.

For the nanofiltration experiments, the salts and neutral solute concentrations were fixed at 0.01 M and 300 ppm, respectively. In this analysis, the neutral solute samples were measured using a total organic carbon analyzer. The NF membranes separation capability was evaluated in terms of Robs and R_{real} based on the following equations as used in the previous report [18] [Equations (2) and (3)]:

$$R_{obs} = \left[1 - \frac{C_p}{C_b}\right] \tag{2}$$

$$R_{real} = \left[1 - \frac{C_p}{C_w}\right] \times 100 \tag{3}$$

where C_p is the salt concentration in permeate, C_b is the salt concentration in bulk and C_w is the salt concentration in wall.

2.4 *Membrane characterizations*

2.4.1 Irreversible thermodynamics model

In general, diffusion and convection components are considered as transport agents in NF membranes. Both components are reflected in the Spiegler-Kedem equation, which comprises diffusion and convection based on Hagen-Poiseuille's law [40]–[43]. Equation (7) is known as the Spiegler-Kedem equation [Equation (4)].

$$J_s = -P\Delta x \frac{dc}{dx} + (1-\sigma) Jvc \tag{4}$$

where J_s is averaged solute flux over membrane surface (mol/m^{2}s), P is permeability (m/s), Δx is membrane thickness (m), σ is reflection coefficient (%), Jv is volume flux (m/s) and c is concentration (mol/m^3) [Equation (5)].

$$J_v = \frac{\varepsilon r}{8\eta\tau} \frac{\Delta P}{\Delta x} \tag{5}$$

where ε is membrane porosity, r is a radius of a stirred cell, η is ratio of solute radius to pore radius, τ is tortuosity and ΔP is applied pressure (Pa) [Equation (6)] .

$$R_i = \left(1 - \frac{C_p, i}{C_r, i}\right) \times 100 \tag{6}$$

where R_i is rejection of component i (%), $C_{p,i}$ is concentration of component i in the permeate (mol/l) and $C_{r,i}$ is concentration of component i in the rejection (mol/l).

$$R_{real} = \left(\frac{\sigma(1-F)}{1-\sigma F}\right) \tag{7}$$

where R_{real} is real rejection, σ is reflection coefficient and F is Faraday constant [Equation (8)].

$$F = \exp\left(-\frac{1-\sigma}{P} J_v\right) \tag{8}$$

2.4.2 SHP model

Steric Hindrance Pore (SHP) model is very important in describing the separation characteristics of nanofiltration membranes and processes. Few membranes parameters that are pore radius (r_p), ratio of thickness to porosity ($\Delta x/A_k$), reflection coefficient (σ), permeability (P_s) and the important steric-hindrance parameters (H_{Di} and H_{Fi}). The analysis of these parameters was modeled and described as in the previous report [30].

2.4.3 TMS model

In Teorell-Meyer-Sievers (TMS) model, a Donnan (electrostatic) factor is one of the main transport mechanisms in NF membranes, and the quantitative analysis of electrostatic properties is very important. Therefore, to quantify and describe these electrostatic

properties, the TMS model was applied. In this model, membrane electrical properties were assumed as fixed circular dispersal of charges and ions [42], [44]. in the previous study [30], TMS model allowed the measurement of σ_{salt}, P_{salt} and the important zeta potential/surface charge (ζ) of the fabricated skinned NF membranes

2.4.4 Pore radius, r_p

Combining with the Spiegler-Kedem equation, the reflection coefficient, σ was determined. Using the relation of $\eta = r_s/r_p$, the membranes' pore radius, r_p and H_F, H_D, S_F and S_D could be measured as described in the previous report [30].

2.4.5 Membranes parameters/properties (P_s, Δx and $\Delta x/A_k$)

Using the measured solute diffusivity as 1.61×10^{-9} m^2/s from the Stokes-Einstein equation, the membranes thickness, porosity and solute permeability could examine based on SHP model as described in the previous report [45], [46].

2.4.6 Electrostatic properties (X_d and ζ)

The electrostatic (Donnan) factors are represented by the membrane surface charge; ζ and charge density, X_d. The determination of these properties was based on the TMS model as described in the previous study [18].

2.4.7 Scanning electron microscopy

The morphologies of the membrane samples were analyzed using scanning electron microscopy (SEM). The principles of operation of SEM is described as follows. A narrow beam of electron with kinetic energy of 1–25 kV hit the membrane sample. The incident electrons are called primary (high-energy) electrons, and those reflected are called secondary electrons. Secondary electrons (low energy) are not reflected but liberated from atoms on the surface; which determine the imaging (what is seen on the screen or the micrograph).

When a membrane is being placed in the electron beam, the sample could be burnt or damaged, depending on the type of polymer and accelerating voltage employed. This could be avoided by coating the membranes with a conducting layer (gold palladium) to prevent them from charging up the surface. Scanning electron microscopy allows a clear view of the overall structure of the membranes; the top surface, the cross-section and the bottom surface could all be observed nicely [47].

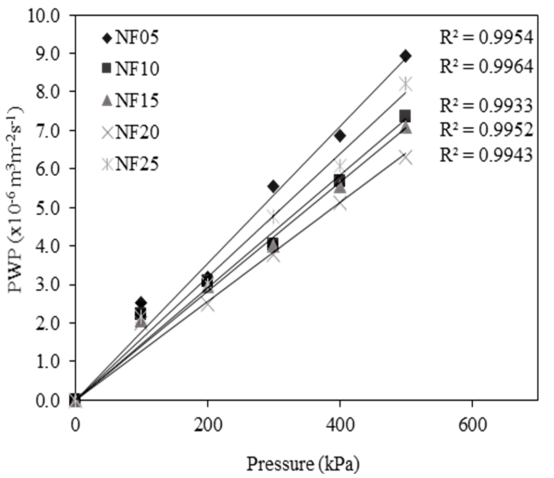

Figure 2: PWP of skinned-oriented nanofiltration membranes.

For the morphological analysis, the samples of membranes were immersed in nitrogen liquid for a few seconds before rupturing cryogenically. The fractured samples were mounted neatly on stubs and coated with a thin layer of gold auto-coater (JFC 1600). The samples were then scanned under JEOL JSM 6360LA Scanning Electron Microscope (Japan) with 10.0 kV potentials and magnitude up to 800X [19], [20].

3 Results and Discussion

3.1 *Performances and separation characteristics*

NF membranes were evaluated in terms of PWP, solute permeation, salt rejection and solutes rejection. Furthermore, the membrane parameters, steric-hindrance factors and key properties were also deduced based on theoretical models. Figure 2 shows the NaCl fluxes data. In general, pure water flux data revealed that the shorter evaporation time the higher PWP was obtained and this trend is linearly increased with the increase of operating pressure.

At 500 kPa, the highest PWP of 8.94×10^{-6} m^3/m^{2}s was demonstrated by the membranes, which were

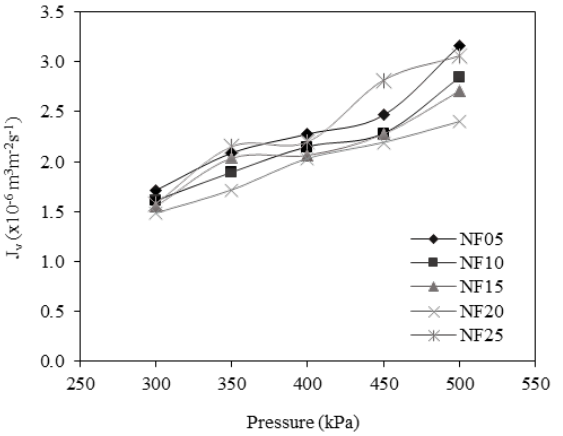

Figure 3: NaCl volume fluxes (0.01 M) of skinned-oriented nanofiltration membranes.

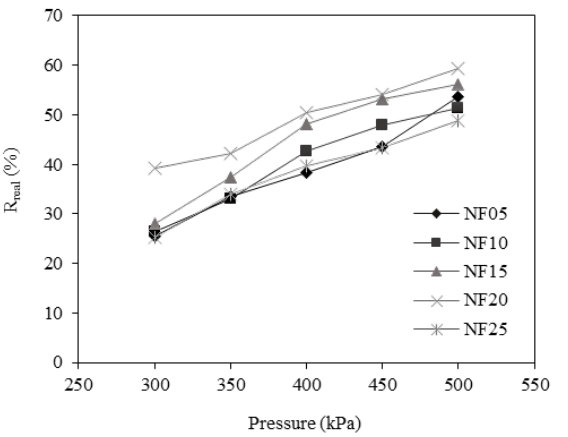

Figure 4: Real rejection, R_{real} of 0.01 M NaCl.

prepared at 5 s (NF05) of evaporation time. However, beyond the 20 s, the membrane prepared at 25 s (NF25) showed the opposing trend of water flux of about 8.21×10^{-6} m^3/m^{2}s was achieved.

Experimental data of volume flux in Figure 3 showed similar trends to PWP. At 500 kPa, the membrane fabricated at 5 s (NF05) of evaporation time shows the highest volume flux of about 3.16×10^{-6} m^3/m^{2}s. From 5 s to 20 s, the volume flux decreased gradually. This trend was similar as described by the previous researchers [48]–[50].

The thickness skin layer could be varied by inducing evaporation time. The increasing of evaporation time was also found to increase the membrane skin layer thickness and these effects are discovered to be the main causes for the reduction of membrane flux. However, beyond 20 s, the volume flux was reached up to 3.06×10^{-6} m^3/m^{2}s. These opposite trends of PWP and volume flux profiles showed the existence of optimum evaporation time.

In Figure 4, the 20 s evaporation time (NF20) membrane showed the highest rejection of about 59.5% while the longest evaporation time membrane (NF25) demonstrated only 46.8% of salt rejection. These results are due to the alteration of membrane's structural properties as described and in agreement with those obtained by the previous researchers [49]–[51]. In their reports, the researchers reported that the increase in evaporation time caused the decrease in pore size. Besides, surface and membranes porosity was also found to be reduced, which was accompanied

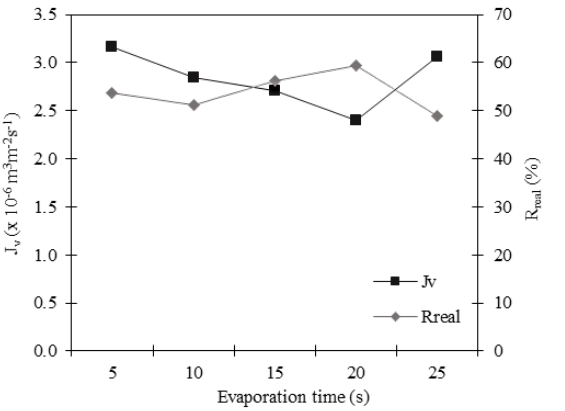

Figure 5: J_v and R_{real} at different evaporation time (0.01 M NaCl and 500 kPa).

by the increase of membranes skin layer thickness with the increase of evaporation time. The pore radius and skin layer are to be reduced. Therefore, with all the properties affected by the evaporation factor, the identification of the optimum evaporation time is essential.

In order to verify and prove the existing of the optimum evaporation time at 20 s, the result of volume and real rejection at 500 kPa was plotted as in Figure 5.

From the graph, it is clearly shown that there are two intersections in between the evaporation time of 10 s to 20 s. At 10 s of evaporation time, the fabricated membranes exhibited an opposing trend of membrane performances. The highest rejection of about 59.4% was achieved by the 20 s membranes (NF20). However, beyond the 20 s, even the volume flux increased, the salt rejection was found to be reduced to only 48.9%. From

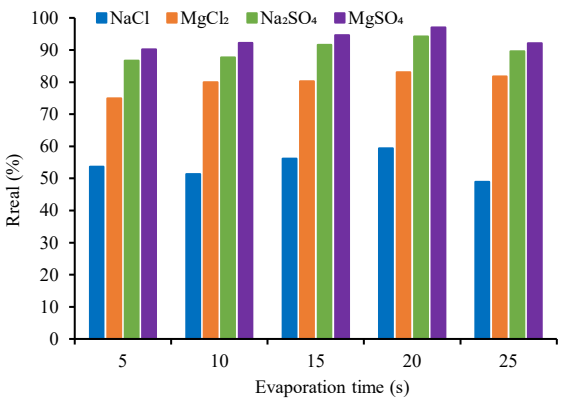

Figure 6: Real rejection, R_{real} of salts at different evaporation time (0.01 M and 500 kPa).

the experimental results, therefore, it was clearly verified that 20 s was found to be the optimum evaporation time for producing highly selective fine NF membranes.

Figure 6 showed the results of multivalent salt rejection. Multivalent salts that are Na_2SO_4, $MgSO_4$, and $MgCl_2$ were used for the performance evaluation at 500 kPa of operating pressure. Generally, the fabricated fine skinned NF membranes demonstrated fine separation capability up to the highest value of 97.02% for $MgSO_4$. For the overall multivalent salts, the highest rejection was demonstrated by the membrane, which was prepared at 20 s.

Similar to the results obtained at different shear rates, the rejection sequences for all membranes were $MgSO_4 > Na_2SO_4 > MgCl_2 > NaCl$ which is explained by the ions diffusion coefficient (D_∞) and solute size (r_s) as shown in Table 2. These factors led towards the specific separation trend in Figure 4 due to the Donnan exclusion factor [52]. Similar trends stated by previous researchers [18], [42], [53].

Table 2: Diffusion coefficient and solute size

Ions	$D_\infty \times 10^{-9}$ (m2s^{-1})	r_s (nm)
Na^+	1.33	0.18
Mg^{2+}	0.70	0.35
Cl^-	2.01	0.12
SO_4^{2-}	1.06	0.23

3.2 *Membranes parameters and structural properties*

Based on the neutral solute separation data, the theoretical models were employed to determine the membranes parameters and structural properties as presented in Table 3. In general, the increase in evaporation time caused the increase in the reflection coefficient parameter. However, from the 15 s and above, the reflection coefficient values gave the constant values. Meanwhile, the membrane permeability exhibited small changes for every solute. As the membrane selectivity is monitored by the structures, pore size and skin layer, this study discovered that pore radius and surface porosity were decreased with the increasing of evaporation time. Besides, the increase in skin layer thickness affects the higher solute permeability and volume fluxes.

The analysis data on the parameters and properties of the NF membranes were shown in Tables 4 and 5. In general, the increase in evaporation time was found to cause an increase in the reflection coefficient. When the highest reflection coefficient of 0.26 reached at the 20 s, the increase of evaporation time beyond the point caused the deterioration of the coefficient to 0.21. In approximately about 19.2% of reduction, these findings revealed that the higher evaporation time beyond the optimum produced the smaller numbers of the small pore size compared to solute size, which is associated with the higher permeation, porosity and pore size as well. As the membranes showed higher rejection, better reflection coefficient and the best results of steric-hindrance factors of HF, SF and SD (1.31, 0.56 and 0.34), therefore these modeling verified that the optimum evaporation time is at 20s.

In Table 5, the highest solute permeability value of about 2.25×10^{-7} m/s was exhibited by the membranes at 25 s. This result supports the above hypothesis that beyond 20 s of the evaporation times the NF membranes exhibited higher permeability due to the reduction in the number of small pores in the membranes. Besides, the membrane pore size of about 0.93 nm at the 25 s (evaporation time) was also found to be larger than the 0.91 nm of pore radius at 20 s. Similar trends were also shown by the values of $\Delta x/A_k$, which proved that the longer evaporation time changes the performance and properties of asymmetric nanofiltration membranes.

As the evaporation time increased, the electrostatic properties of charge density, X_d and surface charge, ζ (zeta potential), were also found to exhibit very positive results. With only about 0.034 mol/m^3 at 5 s,

Table 3: Properties of skinned-oriented nanofiltration membranes

Evaporation Time (s)	Neutral Solutes	Structural Parameters and Properties					
		σ (-)	Ps (10^{-7} ms^{-1})	r_p (nm)	η (r_s/r_p)	$A_k/\Delta x$(m^{-1})	$\Delta x/A_k$ (μm)
5	Glycerol	0.38	3.73	1.11	0.23	817	87.88
	Glucose	0.44	2.59	2.29	0.28	881	77.32
	Saccharose	0.57	1.78	1.18	0.40	1150	54.25
	Raffinose	0.79	0.78	0.89	0.65	1840	18.07
	PEG 1000	0.87	0.37	1.09	0.77	3370	7.94
10	Glycerol	0.39	3.52	1.07	3.52	1.07	0.24
	Glucose	0.45	2.45	1.26	0.29	855	75.55
	Saccharose	0.61	1.60	1.07	0.44	1180	47.23
	Raffinose	0.79	0.68	0.89	0.65	1610	18.07
	PEG 1000	0.89	0.25	0.98	0.80	3000	5.89
15	Glycerol	0.44	2.95	0.92	0.28	733	77.32
	Glucose	0.52	2.05	1.03	0.35	857	63.11
	Saccharose	0.68	1.31	0.91	0.52	1290	35.26
	Raffinose	0.84	0.46	0.81	0.72	1720	11.42
	PEG 1000	0.93	0.12	0.90	0.87	3180	2.57
20	Glycerol	0.44	2.86	0.92	0.28	712	77.31
	Glucose	0.52	2.04	1.04	0.35	851	63.10
	Saccharose	0.68	1.28	0.91	0.52	1270	35.25
	Raffinose	0.86	0.37	0.77	0.75	1750	9.05
	PEG 1000	0.93	0.11	0.90	0.87	3140	2.56
25	Glycerol	0.41	3.05	1.00	0.26	710	82.62
	Glucose	0.51	2.08	1.07	0.34	842	64.89
	Saccharose	0.69	1.25	0.89	0.53	1300	33.60
	Raffinose	0.85	0.43	0.79	0.74	1800	10.21
	PEG 1000	0.93	0.11	0.90	0.87	3120	2.57

Table 4: SHP parameters for skinned-oriented nanofiltration membranes

Membrane Parameters	Evaporation Time (s)				
	5	10	15	20	25
R_{real} (%)	53.65	51.31	56.13	59.38	48.93
η	0.36	0.34	0.39	0.42	0.32
σ	0.20	0.18	0.23	0.26	0.16
H_F	1.23	1.21	1.27	1.31	1.18
S_F	0.65	0.68	0.61	0.56	0.72
S_D	0.41	0.43	0.37	0.34	0.47

Table 5: Membranes structural properties of skinned-oriented nanofiltration membranes

Membrane Properties	Evaporation Time (s)				
	5	10	15	20	25
$P_s \times 10^{-7}$ (ms^{-1})	2.21	2.07	1.82	1.54	2.25
A_k	2.45	2.31	2.68	2.96	2.14
r_p (nm)	1.10	1.06	0.92	0.91	0.93
$\Delta x/A_k$(μm)	7.94	5.89	2.57	2.56	2.57
X_d	0.034	0.032	0.037	0.040	0.031
ζ (-)	1.98	1.88	2.15	2.34	1.75

the membrane's charge density, X_d was found to be increased and up to the highest value of about 0.04 mol/m^3 at the 20 s. At the same time, the largest zeta potential value of –2.34 was also demonstrated by the NF membranes, which were prepared at the 20 s of evaporation time.

At optimum setting, membrane properties, such as rejection, flux, pore radius and membrane charge exhibited great features and characteristics. Therefore, these results verified that the optimum evaporation time occurred at about 20 s. The result of the best skinned NF membranes was compared with the commercial membranes in Table 6. This data revealed that the fabricated NF membranes possess comparable fine characteristics which are in the ranges of commercial NF membranes.

Table 6: Comparison of skinned-oriented membranes with 29 commercial nanofiltration membranes

Properties	r_p (nm)	ζ (-)	$\Delta x/A_k$ (μm)
Minimum	0.39	1.5	0.66
Mean	0.66	9.2	4.8
Maximum	1.59	44.5	16.9
NF20	0.91*	2.34*	2.56*

3.3 *Morphological structures*

In general, the fabricated nanofiltration membranes possess fine asymmetrical structures of skin and sub-layers. Figure 7 showed the morphologies and key properties of nanofiltration membranes fabricated at different evaporation times. In NF20 membranes, smaller finger-like pores were produced at 5 s of the evaporation time. As the time increased to 10 s, the membrane morphologies were changed into denser structures. The finger-like structures were diminished and transformed into small tears-like pores. Since small numbers of macro and micro-voids and spongy structures formed beneath the sub-layer, the membrane's skin layer thickness is also found to be increased. Thus, these might be predominant factors to the improvement of membrane selectivity [18].

As the evaporation time increased, the membrane's skin layer thickness was also found to be increased. This phenomenon is due to the variation in the existence of unoccupied space within the separation process [29]. However, at longer evaporation times from 15 s to 25 s produced better membranes. With good skin layer thickness, the NF15, NF20 and NF25 membranes demonstrated fine morphologies of good finger-likes and tear-likes pores and fine spongy sub-layer, which make the membranes more selective and finer in characters. Previous studies by several researchers discovered that the longer evaporation time formed a homogeneous active layer and more resistive top layer [29], [54].

Based on the experimental, modeling and morphological structures results, the increased evaporation time the thinner skin layer thickness is produced. This factor expanded the nanofiltration membranes to a certain standard of performance. Meanwhile, key properties data revealed that the longer evaporation times produced smaller pore radius as well as denser and thicker skin layer [37]. NF membranes prepared at 20 s demonstrated the smallest

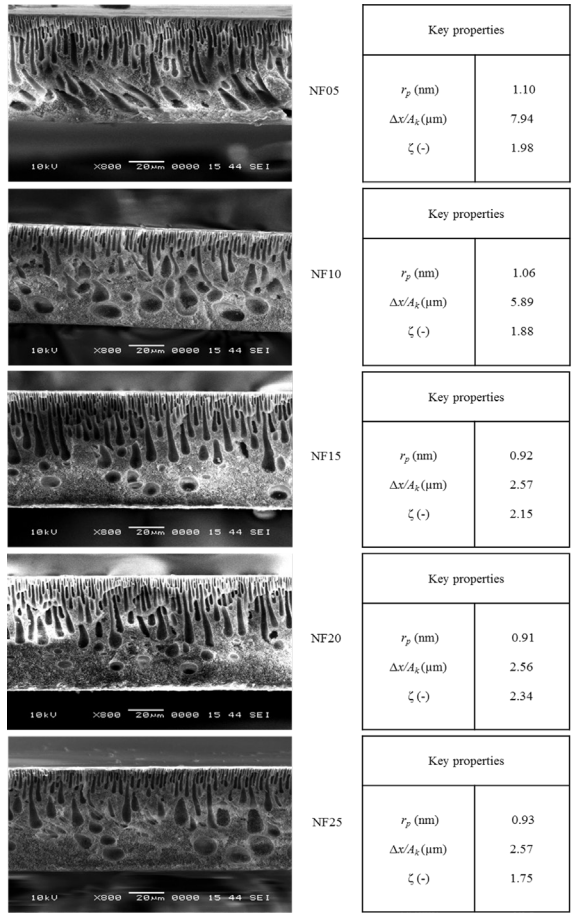

Figure 7: Morphologies and key properties of asymmetric skinned-oriented nanofiltration membranes.

pore radius and finest key properties. Therefore, these analyses verified that the optimum evaporation for the production of fine selective skinned asymmetric nanofiltration membranes was found to be at 20 s.

4 Conclusions

The employing different evaporation times in membranes making during the dry/wet phase inversion membranes making produced the selective skinned-oriented nanofiltration membranes. Experimental data revealed that the evaporation times significantly enhanced the performance and properties of the membrane. The optimum evaporation time for skinned-oriented nanofiltration was found to be at 20 s. Modeling analysis proved that, the nanofiltration membranes produced at

20 s possess the narrowest pores and highest surface charge of about 0.91 nm and 2.34, respectively. Moreover, the increase in evaporation times changes the common asymmetrical morphologies into finer structures with tears-like pores and spongy structures which led to better separation efficacy. Eventually, the technical data of key properties, membranes parameters and structural details from this study are very critical and enable a proper selection of membranes-application matching process.

Acknowledgments

The authors wish to thanks to East Coast Environmental Research Institute and Institute of Oceanography and Environment for their help and analysis guidance.

Author Contributions

A.R.H.: conceptualization, research design, investigation, data curation, reviewing and editing; N.H.M.S.: research design, investigation, methodology, data analysis, writing an original draft; S.R.: data analysis, reviewing and editing; R.O.: conceptualization, data review. All authors have read and agreed to the published this version of the manuscript.

Conflicts of Interest

The authors declare no conflict of interest.

Nomenclature

A_k membrane porosity
c concentration (mol/m^3)
c_b salt concentration in bulk
c_p salt concentration in permeate
$c_{p,i}$ concentration of component i in the permeate (mol/l)
$c_{r,i}$ concentration of component i in the rejection (mol/l)
c_w salt concentration in wall
D_∞ diffusion coefficient
F Faraday constant (96487) (C/mol)
H_D steric parameters related to wall correction factors under diffusion and convection conditions, respectively (-)
H_F steric parameters related to wall correction factors under diffusion and convection conditions, respectively (-)
J_s averaged solute flux over membrane surface (mol/m^{2}s)
J_v volume flux (m/s)
M_w molecular weight (g/mol)
P permeability (m/s)
P_s solute permeability (m/s)
r radius of stirred cell
r_p pore radius (m)
r_s Stokes radius of solute (m), or radius of solute (m or nm)
R_i rejection of component i (%)
R_{obs} observation rejection
R_{real} real rejection
S_D distribution coefficients of solute by steric-hindrance effect under diffusion and convection condition, respectively (-)
S_F distribution coefficients of solute by steric-hindrance effect under diffusion and convection condition, respectively (-)
X_d charge density
ΔP applied pressure (Pa)
Δx membrane thickness (m)
$\Delta x/A_k$ ratio of membrane thickness to membrane porosity

Greek letter
σ reflection coefficient (%)
ε membrane porosity (dimensionless)
η ratio of solute radius to pore radius
τ tortuosity (dimensionless)
ζ zeta potential

References

[1] K. F. M. Yunos, N. A. Mazlan, M. N. M. Naim, A. S. Baharuddin, and A. R. Hassan, "Ultrafiltration of palm oil mill effluent: Effects of operational pressure and stirring speed on performance and membranes fouling," *Environmental Engineering Research*, vol. 24, pp. 263–270, 2019, doi: 10.4491/EER.2018.175.

[2] M. Mirfendereski and T. Mohammadi, "Investigation of H_2S and CO_2 removal from gas streams using hollow fiber membrane gas-liquid contactors," *Chemical and Biochemical Engineering Quarterly*, vol. 31 pp. 139–144, 2017, doi: 10.15255/CABEQ. 2016.1022.

[3] M. J. Regufe, V. V. Santana, A. F. P. Ferreira, A. M.

Ribeiro, J. M. Loureiro, and I. B. R. Nogueira, "A hybrid modeling framework for membrane separation processes: Application to lithium-ion recovery from batteries," *Processes*, vol. 9, 2021, Art. no. 1939, doi: 10.3390/pr9111939.

[4] M. Zebić Avdičević, K. Košutić, and S. Dobrović, "Flux decline study of tubular ceramic and flat sheet UF membranes in textile wastewater treatment," *Chemical and Biochemical Engineering Quarterly*, vol. 33, pp. 405–415, 2019, doi: 10.15255/CABEQ.2018.1570.

[5] S. H. Zainal, A. R. Hassan, and M. H. M. Isa, "The effect of polymer concentration and surfactant types on nanofiltration-surfactant membrane for textile wastewater," *Malaysian Journal of Analytical Science*, vol. 20, pp. 1524–1529, 2016, doi: 10.17576/mjas-2016-2006-34.

[6] S. Wang, X. Li, H. Wu, Z. Tian, Q. Xin, G. He, D. Peng, S. Chen, Y. Yin, Z. Jiang, and M. D. Guiver, "Advances in high permeability polymer-based membrane materials for CO_2 separations," *Energy and Environmental Science*, vol. 9, pp. 1863–1890, 2016, doi: 10.1039/c6ee00811a.

[7] N. A. Sulaiman, A. R. Hassan, S. Rozali, N. H. Mohd Safari, C. W. I. C. W. Takwa, A. D. K. Mansoor A, and M. H. M. Saad, "Development of asymmetric low pressure reverse osmosis-surfactants membrane: Effect of surfactant types and concentration," *Periodica Polytechnica Chemical Engeering*, vol. 64, pp. 296–303, 2020, doi: 10.3311/PPch.13327.

[8] M. A. U. R. Alvi, M. W. Khalid, N. M, Ahmad, M. B. K. Niazi, M. N. Anwar, M. Batool, W. Cheema, and S. Rafiq, "Polymer concentration and solvent variation correlation with the morphology and water filtration analysis of polyether sulfone microfiltration membrane," *Advances in Polymer Technology*, vol. 2019, pp. 1–11, 2019, doi: 10.1155/2019/8074626.

[9] N. Aryanti, D. H. Wardhani, and A. Nafiunisa, "Ultrafiltration membrane for degumming of crude palm oil-isopropanol mixture," *Chemical and Biochemical Engineering Quarterly*, vol. 32, pp. 325–334, 2018, doi: 10.15255/CABEQ.2017.1244.

[10] N. S. M. Ali and A. R. Hassan, "The effect of CTAB and SDS surfactant on the morphology and performance of low pressure active reverse osmosis membrane," *Malaysian Journal of Analytical Science*, vol. 20, pp. 510–516, 2016, doi: 10.17576/mjas-2016-2003-07.

[11] M. Sadrzadeh and S. Bhattacharjee, "Rational design of phase inversion membranes by tailoring thermodynamics and kinetics of casting solution using polymer additives," *Journal of Membrane Science*, vol. 441, pp. 31–44, 2013, doi: 10.1016/j.memsci.2013.04.009.

[12] A. R. Hassan, S. Rozali, N. H. M. Safari, and B. H. Besar, "The roles of polyethersulfone and polyethylene glycol additive on nanofiltration of dyes and membrane morphologies," *Environmental Engineering Research*, vol. 23, pp. 316–322, 2018, doi: 10.4491/eer.2018.023.

[13] L. Gao, B. Tang, and P. Wu, "An experimental investigation of evaporation time and the relative humidity on a novel positively charged ultrafiltration membrane via dry-wet phase inversion," *Journal of Membrane Science*, vol. 326, pp. 168–177, 2009, doi: 10.1016/j.memsci.2008.09.048.

[14] N. A. Ali, A. R. Hassan, and L. Y. Wong, "Development of novel asymmetric ultra low pressure membranes and a preliminary study for bacteria and pathogen removal applications," *Desalination*, vol. 206, pp. 474–484, 2007, doi: 10.1016/j.desal.2006.02.074.

[15] S. Li, Z. Cui, L. Zhang, B. He, and J. Li, "The effect of sulfonated polysulfone on the compatibility and structure of polyethersulfone-based blend membranes," *Journal of Membrane Science*, vol. 513, pp. 1–11, 2016, doi: 10.1016/j.memsci.2016.04.035.

[16] N. I. M. Fadilah and A. R. Hassan, "Preparation, characterization and performance studies of active pvdf ultrafiltration-surfactants membranes containing PVP as additive," *Malaysian Journal of Analytical Sciences*, vol. 20, pp. 335–341, 2016.

[17] A. R. Hassan and M. S. A. Munaim, "Fabrication and characterization of integrally skinned-oriented highly selective charged asymmetric low pressure poly(ether sulfone) membranes for nanofiltration," *Journal of Chemical Technology and Biotechnology*, vol. 87, pp. 559–569, 2011, doi: 10.1002/jctb.2751.

[18] A. F. Ismail and A. R. Hassan, "Effect of additive contents on the performances and structural

properties of asymmetric polyethersulfone (PES) nanofiltration membranes," *Separation and Purification Technology*, vol. 55, pp. 98–109, 2007, doi: 10.1016/j.seppur.2006.11.002.

[19] N. H. M. Safari, A. R. Hassan, C. W. I. C. W. Takwa, and S. Rozali, "Deduction of surfactants effect on performance, morphology, thermal and molecular properties of polymeric polyvinylidene fluoride (PVDF) based ultrafiltration membrane," *Periodica Polytechnica Chemical Engineering*, vol. 63, pp. 27–35, 2019, doi: 10.3311/PPch.12423.

[20] A. R. Hassan, C. W. I. C. W. Takwa, N. H. M. Safari, S. Rozali, and N. A. Sulaiman, "Characterization on performance, morphologies and molecular properties of dual-surfactants based polyvinylidene fluoride ultrafiltration membranes," *Periodica Polytechnica Chemical Engineering*, vol. 64, pp. 320–327, 2020, doi: 10.3311/PPch.13862.

[21] Y. Yurekli, "Removal of heavy metals in wastewater by using zeolite nano-particles impregnated polysulfone membranes," *Journal of Hazardous Materials*, vol. 309, pp. 53–64, 2016, doi: 10.1016/j.jhazmat.2016.01.064.

[22] K. Hendrix, G. Koeckelberghs, and I. F. J. Vankelecom, "Study of phase inversion parameters for PEEK-based nanofiltration membranes," *Journal of Membrane Science*, vol. 452, pp. 241–252, 2014, doi: 10.1016/j.memsci.2013.10.048.

[23] A. S. M. Ali, E. A. Fadl, M. M. Soliman, and S. H. Kandil, "Optimization of the evaporation step in cellulose acetate membranes preparation by dry–wet phase inversion technique for water desalination applications," *Desalination and Water Treatment*, vol. 174, pp. 63–70, 2020, doi: 10.5004/dwt.2020.24862.

[24] Y. Zhang, J. Sunarso, S. Liu, and R. Wang, "Current status and development of membranes for CO_2/CH_4 separation: A review," *International Journal of Greenhouse Gas Control*, vol. 12, pp. 84–107, 2013, doi: 10.1016/j.ijggc.2012.10.009.

[25] S. C, Pesek and W. J. Koros, "Aqueous quenched asymmetric polysulphone hollow fibers prepared by dry/wet phase separation," *Journal of Membrane Science*, vol. 88, pp. 1–19, 1994, doi: 10.1016/0376-7388(93)E0150-I.

[26] S. Hao, J. Wen, S. Li, J. Wang, and Z. Jia, "Preparation of COF-LZU1/PAN membranes by an evaporation/casting method for separation of dyes," *Journal of Materials Science*, vol. 55, pp. 14817–14828, 2020, doi: 10.1007/s10853-020-05090-8.

[27] W. N. R. Jami'an, H. Hasbullah, F. Mohamed, N. Yusof, N. Ibrahim, and R. R. Ali, "Effect of evaporation time on cellulose acetate membrane for gas separation," in *IOP Conference Series: Earth and Environmental Science*, 2016, vol. 36, Art. no. 012008.

[28] X. Y. Chen, H. Vinh-Thang, A. A. Ramirez, D. Rodrigue, and S. Kaliaguine, "Membrane gas separation technologies for biogas upgrading," *RSC Advances*, vol. 5, pp. 24399–24448, 2015, doi: 10.1039/c5ra00666j.

[29] H. B. Park, J. Kamcev, L. M. Robeson, M. Elimelech, and B. D. Freeman, "Maximizing the right stuff: The trade-off between membrane permeability and selectivity," *Science*, vol. 356, no. 6343, 2017, doi: 10.1126/science.aab0530.

[30] S. Rozali, N. H. M. Safari, A. R. Hassan, M. Ahmad and R. M. Yunus, "Assessment on performance-properties of asymmetric nanofiltration membranes from polyethersulfone/n-methyl-2-pyrrolidone/water blends with poly(Vinyl pyrrolidone) as additive," *Periodica Polytechnica Chemical Engineering*, vol. 1, pp. 54–69, 2022, doi: 10.3311/PPch.18357.

[31] T. Tavangar, M. Karimi, M. Rezakazemi, and K. Raghava, "Textile waste, dyes/inorganic salts separation of cerium oxide-loaded loose nanofiltration polyethersulfone membranes," *Chemical Engineering Journal*, vol. 385, 2020, Art. no. 123787, doi: 10.1016/j.cej.2019.123787.

[32] Q. Long, Z. Zhang, G. Qi, Z. Wang, Y. Chen, and Z. Liu, "Fabrication of chitosan nanofiltration Membranes by the film casting strategy for effective removal of dyes/salts in textile wastewater," *ACS Sustainable Chemical and Engineering*, vol. 8, pp. 2512–2522, 2020, doi: 10.1021/acssuschemeng.9b07026.

[33] S. Zinadini, A. A. L. Zinatizadeh, M. Rahimi, and V. Vatanpour, "Magnetic field-augmented coagulation bath during phase inversion for preparation of $ZnFe_2O_4$/SiO_2/PES nanofiltration membrane: A novel method for flux enhancement and fouling resistance," *Journal of Industrial and Engineering Chemistry*, vol. 46, pp. 9–18, 2017, doi: 10.1016/j.jiec.2016.08.005.

[34] D. Guo, Y. Xiao, T. Li, Q. Zhou, L. Shen, R. Li, Y. Xu, and H. Lin, "Fabrication of highperformance composite nanofiltration membranes for dye wastewater treatment: mussel-inspired layer-by-layer self-assembly," *Journal of Colloid and Interface Science*, vol. 560, pp. 273–283, 2020, doi: 10.1016/j.jcis.2019.10.078.

[35] J. Wu, M. Xia, Z. Li, L. Shen, R. Li, M. Zhang, Y. Jiao, Y. Xu, and H. Lin, "Facile preparation of polyvinylidene fluoride substrate supported thin film composite polyamide nanofiltration: Effect of substrate pore size," *Journal of Membrane Science*, vol. 638, 2021, Art. no. 119699, doi: 10.1016/j.memsci.2021.119699.

[36] J. M. Gohil and R. R. Choudhury, "Introduction to nanostructured and nano-enhanced polymeric membranes: Preparation, function, and application for water purification," in *Nanoscale Materials in Water Purification*. Amsterdam, Netherland: Elsevier, 2019, pp. 25–57, doi: 10.1016/B978-0-12-813926-4.00038-0.

[37] Y. H. See-Toh, F. C. Ferreira, and A. G. Livingston, "The influence of membrane formation parameters on the functional performance of organic solvent nanofiltration membranes," *Journal of Membrane Science*, vol. 299, pp. 236–250, 2007, doi: 10.1016/j.memsci.2007.04.047.

[38] A. F. ismail and A. R. Hassan, "Formation and characterization of asymmetric nanofiltration membrane: Effect of shear rate and polymer concentration," *Journal of Membrane Science*, vol. 270, pp. 57–72, 2006, doi: 10.1016/j.memsci.2005.06.046.

[39] S. C. Pesek and W. J. Koros, "Aqueous quenched asymmetric polysulfone membranes prepared by dry/wet phase separation," *Journal of Membrane Science*, vol. 81, pp 71–88, 1993, doi: 10.1016/0376-7388(93)85032-R.

[40] V. A. Montesdeoca, A. E. Janssen, R. M. Boom, and A. Van der Padt, "Fine ultrafiltration of concentrated oligosaccharide solutions–Hydration and pore size distribution effects," *Journal of Membrane Science*, vol. 580, pp. 161–176, 2019. doi 10.1016/j.memsci.2019.03.019.

[41] Y. Roy and J. H. Lienhard, "On the presence of solute-solvent transport coupling in reverse osmosis," *Journal of Membrane Science*, vol. 611, 2020, Art. no. 118272, doi:10.1016/j.memsci.2020.118272.

[42] M. M. Lorente-Ayza, S. Mestre, M. Menéndez, and E. Sánchez, "Comparison of extruded and pressed low cost ceramic supports for microfiltration membranes," *Journal of the European Ceramic Society*, vol. 35, pp. 3681–3691, 2015, doi: doi:10.1016/j.jeurceramsoc.2015.06.010.

[43] A. Pisano, "From tubes and catheters to the basis of hemodynamics: Viscosity and Hagen–Poiseuille equation," in *Physics for Anesthesiologists and Intensivists*. Cham, Switzerland: Springer, 2021, pp. 89–98.

[44] D. V. Lebedev, V. S Solodovnichenko, M. M. Simunin, and I. I. Ryzhkov, "Effect of electric field on ion transport in nanoporous membranes with conductive surface," *Petroleum Chemistry*, vol. 58, pp. 474–481, 2018, doi: 10.1134/S0965544118060075.

[45] I. I. Ryzhkov and A. V. Minakov, "Theoretical study of electrolyte transport in nanofiltration membranes with constant surface potential/charge density," *Journal of Membrane Science*, vol. 520, pp. 515–528, 2016, doi: 10.1016/j.memsci.2016.08.004.

[46] E. Wallace, J. Cuhorka, and P. Mikulášek, "Characterization of nanofiltration membrane and its practical use for separation of zinc from wastewater," *Waste Forum*, vol. 3, pp. 314–325, 2018.

[47] N. I. M. Fadilah, "Effect of surfactants on pore structure and pore properties of phase inversion ultrafiltration (UF) membrane," M.S. thesis, Faculty of Science and Technology, Universiti Sains Islam Malaysia, Malaysia, 2015.

[48] S. R. Panda and S. De, "Preparation, characterization and performance of $ZnCl_2$ incorporated polysulfone (PSF)/polyethylene glycol (PEG) blend low pressure nanofiltration membrane," *Desalination*, vol. 347, pp. 52–65, 2014, doi:10.1016/j.desal.2014.05.030.

[49] L. García-Fernández, M. C. García-Payo, and M. Khayet, "Effects of mixed solvents on the structural morphology and membrane distillation performance of PVDF-HFP hollow fiber membranes," *Journal of Membrane Science*, vol. 468, pp. 324–338, 2014, doi:10.1016/j.memsci.2014.06.014.

[50] A. K. Hołda, B. Aernouts, W. Saeys, and I. F.

Vankelecom, "Study of polymer concentration and evaporation time as phase inversion parameters for polysulfone-based SRNF membranes," *Journal of Membrane Science*, vol. 442, pp. 196–205, 2013, doi: 10.1016/j.memsci.2013.04.017.

[51] I. Soroko, M. P. Lopes, and A. Livingston, "The effect of membrane formation parameters on performance of polyimide membranes for organic solvent nanofiltration (OSN): Part A. Effect of polymer/solvent/non-solvent system choice," *Journal of Membrane Science*, vol. 381, pp. 152–162, 2011, doi: 10.1016/j.memsci.2011.07.027.

[52] A. Szymczyk, C. Labbez, P. Fievet, A. Vidonne, A. Foissy, and J. Pagetti "Contribution of convection, diffusion and migration to electrolytes transport through nanofiltration membranes," *Advances in Colloid and Interface Science*, vol. 103, pp. 77–94, 2003 doi: 10.1016/S0001-8686(02)00094-5.

[53] J. Kamcev, D. R. Paul, G. S. Manning, and B. D. Freeman, "Predicting salt permeability coefficients in highly swollen, highly charged ion exchange membranes," *ACS Applied Materials and Interfaces*, vol. 9, pp. 4044–4056, 2017, doi: 10.1021/acsami.6b14902.

[54] A. K. Hołda and I. F. J. Vankelecom, "Understanding and guiding the phase inversion process for synthesis of solvent resistant nanofiltration membranes," *Journal of Applied Polymer Science*, vol. 132, no. 27, 2015, Art. no. 42130, doi: 10.1002/app.42130.